Analytica Chimica Acta 1275 (2023) 341378

Contents lists available at ScienceDirect

Analytica Chimica Acta

journal homepage: www.elsevier.com/locate/aca

A microfluidic biosensor architecture for the rapid detection of COVID-19

Sura A. Muhsin [a,1], Ying He [b,c,d,1], Muthana Al-Amidie [a], Karen Sergovia [b,c,d], Amjed Abdullah [a], Yang Wang [b,c,d], Omar Alkorjia [a], Robert A. Hulsey [e], Gary L. Hunter [f], Zeynep K. Erdal [f], Ryan J. Pletka [g], Hyleme S. George [e], Xiu-Feng Wan [a,b,c,d,**], Mahmoud Almasri [a,*]

[a] Department of Electrical Engineering and Computer Science, College of Engineering, University of Missouri, 411 S 6th St, Columbia, Mo, 65211, USA
[b] Center for Influenza and Emerging Infectious Diseases, Department of Molecular Microbiology and Immunology, School of Medicine, Bond Life Sciences Center, University of Missouri, 1201 Rollins St, Columbia, MO, 65211, USA
[c] Department of Molecular Microbiology and Immunology, School of Medicine, University of Missouri, Columbia, MO, USA
[d] Bond Life Sciences Center, University of Missouri, Columbia, MO, USA
[e] Black and Veatch, 11401 Lamar, Overland Park, KS, 66211, USA
[f] Black and Veatch, 201 Brookfield Parkway, Suite 150, Greenville, SC, 29607, USA
[g] Black and Veatch, 2999 Oak Road, Suite 490, Walnut Creek, CA, 94597, USA

HIGHLIGHTS

- The biosensor was able to detect SARS-COV-2 in clinical sample with a concentration as low as 26 TCID50/ml in 40 min.
- The focusing and trapping electrode pairs maximized the number of captured viruses on top of the detection electrode, improving the detection sensitivity.
- Detection of SARS-COV-2 virus with high specificity and selectivity.

GRAPHICAL ABSTRACT

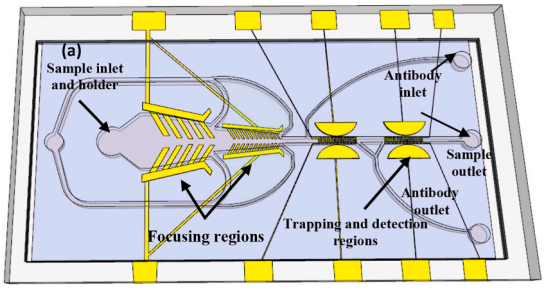

ARTICLE INFO

Handling Editor: Dr. J.P. Landers

Keywords:
Dielectrophoresis
SARS-COV-2
Biosensor
Impedance measurement
Microfluidic
Trapping and focusing electrodes
Polymerase chain reaction (PCR)

ABSTRACT

The lack of enough diagnostic capacity to detect severe acute respiratory syndrome coronavirus 2 (SARS-COV-2) has been one of the major challenges in the control the 2019 COVID pandemic; this led to significant delay in prompt treatment of COVID-19 patients or accurately estimate disease situation. Current methods for the diagnosis of SARS-COV-2 infection on clinical specimens (e.g. nasal swabs) include polymerase chain reaction (PCR) based methods, such as real-time reverse transcription (rRT) PCR, real-time reverse transcription loop-mediated isothermal amplification (rRT-LAMP), and immunoassay based methods, such as rapid antigen test (RAT). These conventional PCR methods excel in sensitivity and specificity but require a laboratory setting and typically take up to 6 h to obtain the results whereas RAT has a low sensitivity (typically at least 3000 TCID50/ml) although with the results with 15 min. We have developed a robust micro-electro-mechanical system (MEMS)

* Corresponding author. Department of Electrical Engineering and Computer Science, College of Engineering, University of Missouri, 411 S 6th st., Columbia, Mo, 65211, USA.
** Corresponding author. Department of Electrical Engineering and Computer Science, College of Engineering, University of Missouri, 411 S 6th st., Columbia, Mo, 65211, USA.
E-mail addresses: wanx@missouri.edu (X.-F. Wan), almasrim@missouri.edu (M. Almasri).
[1] Equal contribution.

https://doi.org/10.1016/j.aca.2023.341378
Received 26 March 2023; Accepted 15 May 2023
Available online 9 June 2023

based impedance biosensor fit for rapid and accurate detection of SARS-COV-2 of clinical samples in the field with minimal training. The biosensor consisted of three regions that enabled concentrating, trapping, and sensing the virus present in low quantities with high selectivity and sensitivity in 40 min using an electrode coated with a specific SARS-COV-2 antibody cross-linker mixture. Changes in the impedance value due to the binding of the SARS-COV-2 antigen to the antibody will indicate positive or negative result. The testing results showed that the biosensor's limit of detection (LoD) for detection of inactivated SARS-COV-2 antigen in phosphate buffer saline (PBS) was as low as 50 TCID50/ml. The biosensor specificity was confirmed using the influenza virus while the selectivity was confirmed using influenza polyclonal sera. Overall, the results showed that the biosensor is able to detect SARS-COV-2 in clinical samples (swabs) in 40 min with a sensitivity of 26 TCID50/ml.

1. Introduction

In December 2019, an infection outbreak caused by a bat-origin novel coronavirus COVID-19 or SARS-COV-2 was detected in Wuhan China [1] Within <3 months [2,3], COVID-19 has spread across China and worldwide, including the United States; on March 11, 2020, the World Health Organization declared the COVID-19 a global pandemic. As July 25 of 2022, the ongoing COVID-19 pandemics have caused >570 million laboratories confirmed infections worldwide, of which >6.38 million were fatal. A total of >1.02 million deaths were estimated to be caused by COVID-19 in the United States alone [4,5], With the concentrating efforts on flattening the currently experiencing (the first) wave, this pandemic expects to cause multiple waves and remains to become an endemic disease in the future [6].

The majority of the currently FDA-approved tests to detect COVID viruses are nucleic acid-based on methods [7,8], and monoclonal antibody based rapid antigen test (RAT). The PCR based methods, such as real-time RT-PCR and real-time RT-LAMP excel in sensitivity and specificity but require a laboratory setting and typically take up to 6 h to obtain the results [9]. Recently, Abbott Diagnostics released a nucleic acid-sequence based method that requires as short as 15 min; however, the data for sensitivity and specificity is still not publicly available. Nevertheless, these nucleotide-based methods can easily suffer the limitations in cross-contaminations and in potential false negative results due to rapid mutations in viruses, especially RNA viruses such as COVID-19 [10,11], RAT, particularly the strip paper, is a rapid immunoassay with the results acquired within approximately 15 min and has been widely for self-test. However, RAT can reliably detect viral loads in the clinical samples with 3000 TCID50/ml [12] thus cannot detect viruses during early stage of diseases and thus can miss the important time for patient care and to block virus transmission. We have been excited that multiple diagnosis platforms were released for COVID-19 in the past several months that can diagnose the virus [13]. Serological tests are not good enough for rapid detection because of the long delay between infection and seroconversion [14]. On the other hand, antibody-based testing is rapid and reliable to identify infection. A countless number of groups have investigated various diagnostic techniques for point-of-care (POC) as well as self-detection kits, e.g., Lateral Flow Immunochromatographic Assay Strips (LFICS) kits that have been extensively used due to ease of use [15]. However, the sensitivity of these kits depends on period of time between infection and testing to produce and detectable response of IgM [16,17].

Alternative diagnostics techniques for detection of SARS-CoV-2 antigen include electrochemical immunosensors based on, e.g., screen-printed electrodes with absorbing cotton padding with LOD of 0.8 pg/mL indicating very good sensitivity [18]; piezoelectric to detect SARS-CoV-2 antigen in just 15 min [19], nucleic acid [20]. Although the nucleic acid-based sensor has good sensitivity, it requires extraction of RNA and trained personnel; optical sensors based on, e.g., surface plasmon resonance to measure the changes of refractive index between different antigen concentrations with a resolution of 3.75×10^{-8} RIU [21], a U-shaped plastic optical fiber sensor has been investigated for the detection of the SARS-CoV-2 in 15 min [22]. In addition, nanomaterial-based sensors such as graphene, metal oxides, and quantum dots, have been investigated for their potential use in the detection of SARS-CoV-2 antigen. These sensors offer advantages such as high sensitivity, and rapid detection for on-site testing [23].

The diagnostic method developed and covered in this paper aims to detect the SARS-COV-2 virus in clinical samples. Given current testing limitations, it becomes clear a more sensitive, real time, field deployable detection method is urgently needed to make testing reliable and practical, which could have an enormous impact on the virus surveillance.

2. Materials and methods

2.1. Design and modelling of the biosensor

A novel microfluidic biosensor based on impedance change measurements was investigated for rapid diagnostic of SARS-COV-2 virus. The biosensor consisted of multiple horizontal fluidic microchannels to concentrate, trap, and sense the virus. Three dimensional (3D) schematics of the biosensor are shown in Fig. 1(a).

The first region has used an electrical focusing mechanism to concentrate the viruses into the centerline of the microchannel and directed them toward the sensing region while the virus free solution, i.e., >90% volume of the original sample media, exited the focusing microchannel via the outer four microchannels into the waste outlet. This design resulted in a significant increase in the sensing sensitivity and achieving low limit of detection (LoD). The focusing region consisted of two sets of ramp down rectangular prism shaped electrode pairs along with thin film finger pairs tilted with 45°. The two sets were connected in a parallel configuration, inside a single horizontal fluidic microchannel, and had lengths of 1 mm and 2 mm, and widths at the beginning and end of the focusing sets of 3.6 mm and 1.2 mm, and 630 μm and 210 μm, respectively. The rectangular prisms were made using electroplated gold (Au) with a height of 15 μm while the tilted fingers were made using chromium (Cr) and gold (Au) thin films with thicknesses of 50 nm and 150 nm, respectively. This design generated positive dielectrophoretic (p-DEP) forces and a high E-field gradient, by applying a modulated voltage, to concentrate the viruses into the centerline of the microchannel, before directing the viruses enriched sample flow toward the sensing microchannel. The thin film finger's width and spacing between them, and the spacing between the inner edges of the finger pairs were 10 μm, and 10 μm, 10 μm, respectively, while the finger width was varied due to the use of ramp down microchannel. In addition, the ramp down feature may marginally aid the focusing process due to the hydrodynamic forces. To determine electrode pairs dimensions with the highest sensitivity, COMSOL Multiphysics software was used for simulation and modeling, as shown in Fig. 2(a).

The second region has used an electrical trapping mechanism to trap the viruses on top of the sensing electrode array. This region consisted of half 3-dimensional (3D) ellipsoid shaped trapping electrode pairs with a fixed height of 15 μm, embedded in SU8 photoresist and surrounded the sensing interdigitated microelectrode (IDE) arrays. This region generated p-DEP forces to trap the viruses on top of the IDE array. It has maximized the virus concentration trapped on top of the sensing electrodes and thus facilitated the contact and binding of the virus antigen

with the antibodies. The trapping electrode pairs were only turned on during the binding process for 30 min. The electrode pairs were designed to generate a non-uniform E-field intensity and gradient, using a modulated voltage source at a specific frequency, with their highest between the trapping electrode pairs across the channel's width and height. The E-field intensity and gradient were decreased significantly along the microchannel's length away from the trapping region, as shown in Fig. 2(b). The applied voltage at a specific frequency polarized the viruses such that they exhibited p-DEP behavior. Thus, they were forced to be trapped on top of the sensing IDE array. This electrode was also simulated using COMSOL.

The third region has used an E-field to sense the viruses. It consisted of a narrow fluidic microchannel with a width of 70 μm housing two sets of IDE arrays, each with 20 finger pairs. The IDE finger width and spacing between the fingers were 5 μm and 3 μm, respectively. Initially, one of the two IDE electrode arrays was functionalized with a specific antibody cross-linker mixture, via the antibody inlets while avoiding contaminating the focusing electrodes and the second set of IDE array that was used as a control electrode. We have prevented the contamination by designing the microchannels with fluid flow control that

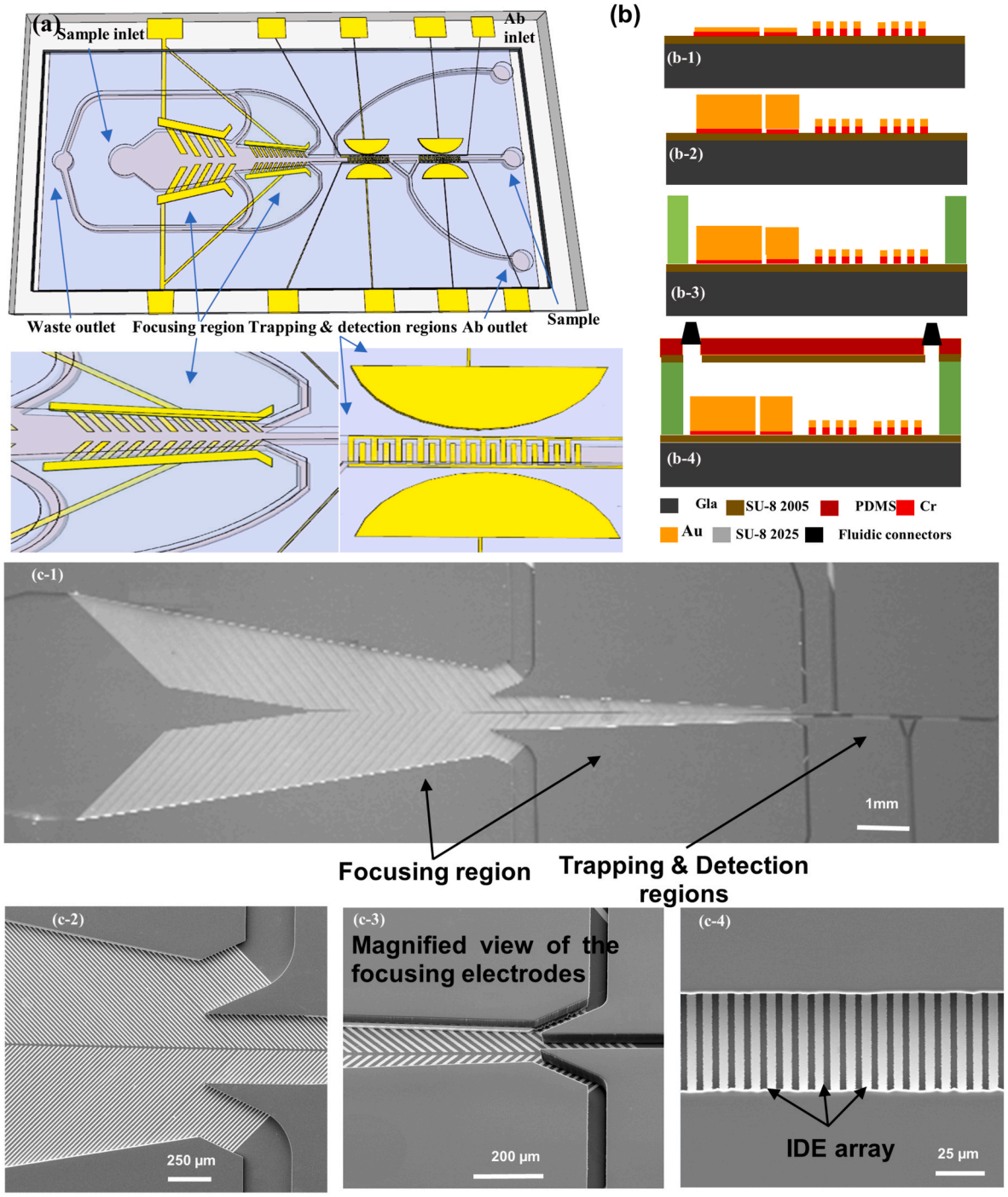

Fig. 1. (a) An electric field (E-Field) modeling and simulation using COMSOL Multiphysics software of the three regions making the biosensor, i.e., (b) focusing, (c) detection regions and (d) tapping (e) An equivalent electrical circuit of the biosensor was also included in the simulation. (f) Finally, experimental and simulation results were obtained after the SARA- Covid-19 antibody-antigen binding occurred in the microchannel.

specified the fluid path during coating the antibody. The control electrode array was not coated or contaminated with antibody. The testing sample was introduced from the sample inlet into the focusing region and once the sensing microchannel was filled with the sample, the flow was stopped for 30 min so that the virus antigen can bind to its specific antibody. This region was also simulated using COMSOL, as shown in Fig. 2(c and d).

The modeling results showed that the miniaturized dimensions significantly increase the impedance measurement sensitivity. The fluidic microchannel was fabricated with a height of 50 μm.

2.2. Equivalent circuit

The impedance response of the biosensor has been examined by creating a model of an equivalent electrical circuit that represents the IDE array's impedance response, as shown in Fig. 2 (e). An electrical circuit model was created to represent the biosensor's impedance response. The model consisted of two components, the solution resistance (R_S) and the double-layer capacitance (CDL), which were proportional to the solution resistivity (ρ_S) and connected in series. The IDE array's impedance response was simulated when the corresponding SARS-COV-2 antibody on the detection electrode's surface bound with the SARS-COV-2 antigen in the PBS solution. When an AC voltage was applied to the IDE array, the equivalent resistance of the solution (R_S) was generated. The dielectric capacitance of SARS-COV-2 (CCOVID-19) was also generated and connected in parallel with both C_{DL} and R_S. The capacitance of CCOVID-19 is influenced by the dielectric constant of the solution and the structure of the detection IDE array. The electrical wiring can also impact the electrical circuit, but this was disregarded because the component's values were insignificant compared to other components in the circuit. Thus, the equivalent circuit's total impedance value comprises the RS and the impedance of the two capacitors, CDL.

The RS, generated when an AC voltage is applied and current flows through the circuit, can be calculated.

$$R_S = \frac{v}{I}\rho_S\frac{D}{A}$$

where A is the surface area of the detection electrode, D is the spacing between the interdigitated fingers, and ρ is the solution resistivity. The total impedance of the equivalent circuit is given by

$$Z_{Dl} = 2Z_{Dl} + R_s$$

$$Z_{Dl} = {}^{1}/_{i\omega COVID-19}$$

$$C_{\mathrm{COVID-19}} = \frac{\varepsilon_r\varepsilon_0 A}{D}$$

Where ε_0 and ε_r are the vacuum permittivity and the solution relative permittivity, respectively, ω is an angular frequency (in radians per second). An EIS spectrum analyzer was employed to examine the equivalent electrical circuit response when a testing solution filled the detection microchannel. The values of COVID-19 and R_S were determined to be 23.6 nF and 10.05 MΩ, respectively, for the SARS-COV-2 antigen, depending on the sample concentration. The high

R_S value was due to the significant number of SARS-COV-2 antigens that had attached to the SARS-COV-2 antibodies on the electrodes. he results indicated that the resistance of the SARS-COV-2 antigen had a more significant impact on the impedance value at low frequencies, while the dielectric capacitance had a minor impact. This suggested that the number of SARS-COV-2 antigens in the solution was the primary cause of the impedance response variation. Moreover, the impedance value remained constant with frequency, except for a low impedance at high frequencies, which was attributed to the antibody-antigen binding.

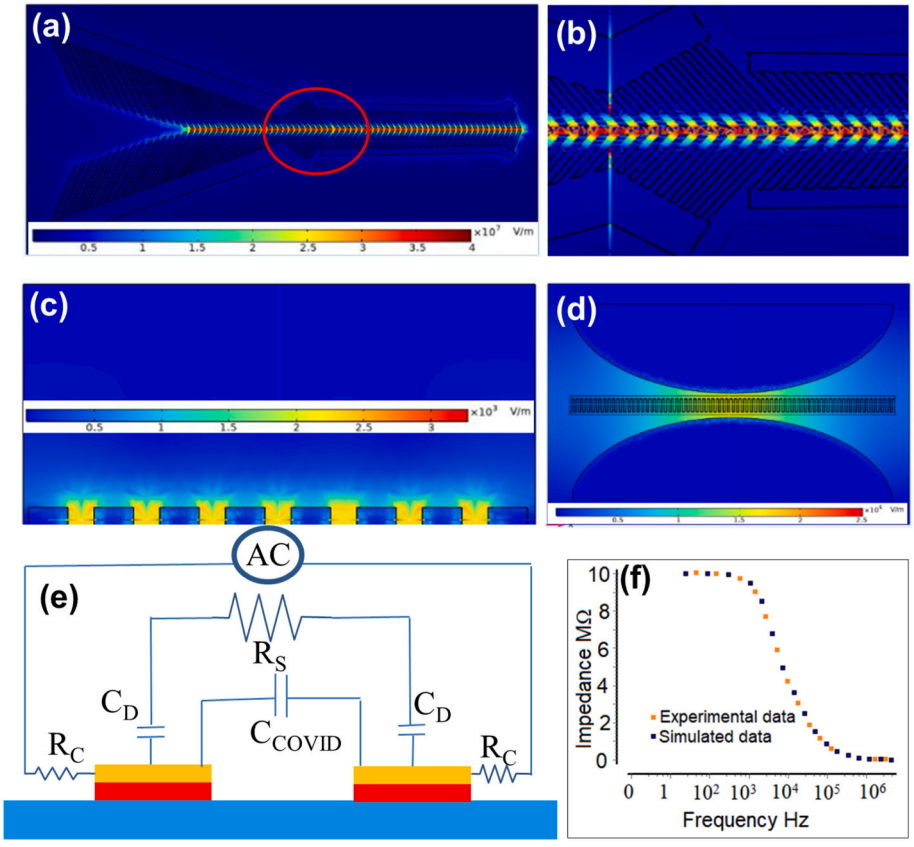

Fig. 2. (a) Three-dimensional (3D) Schematics of the biosensor, presenting the focusing, trapping and detection regions, (b) A side view of biosensor showing the materials used in device fabrication, (c) Scanning electron microscope (SEMs) micrographs of the fabricated biosensor.

Fig. 2 (f) showed that the impedance value was dependent on the dielectric capacitance at higher frequencies, with no impact from the SARS-COV-2 antigen. Therefore, a frequency range of 100 Hz to 1 MHz was used to obtain an acceptable Bode plot. The equivalent circuit model confirmed that the impedance change had the appropriate characteristics, and no machine learning was employed at this stage. However, machine learning will be implemented in future phases of the project.

2.3. Fabrication of the biosensor

The impedance-based microfluidic biosensors were micromachined on glass substrates using thin film, electroplated gold (Au), SU8 negative photoresist, and Polydimethylsiloxane (PDMS) silicone material. The fabrication was performed using surface micromachining technology in the following steps and are shown in Fig. 1 (a). The glass substrates were cleaned with piranha solution for 5 min to remove any existing organic residues and/or contaminants. The piranha solution is a mixture of hydrogen peroxide (H_2O_2) and sulfuric acid (H_2SO_4) with a ratio of 1:3. The substrates were then cleaned with deionized (DI) water for 2 min and blown dry with nitrogen. To fabricate reliable biosensors, a layer of negative photoresist (SU8-2005) with a thickness of 3 μm was spin coated on the substrate, prebaked on two hotplates at 65 °C for 1 min, and 95 °**C** for 2 min. The SU8 was left overnight (>24 h) in order to reduce its stickiness. This is followed by an ultraviolet (UV) flood exposure for 10 s, post baking at 65 °C for 1 min and 95 °C for 1 min. The substrate was then hard baked at 150 °C for 30 min to harden the photoresist thin layer.

To create and pattern the thin film electrodes for focusing, trapping, and sensing, and the seed layer for electroplating the vertical sidewall of the focusing and trapping electrodes, Cr/Au thin films were deposited using an electron beam (e-beam) evaporator. The Au thin film was patterned using Shipley 1805 photoresist and wet etched using a gold etchant solution (Techni gold 25 ES RTU). The Cr layer was used to allow continuous DC current flow to enable uniform electroplating across all desired regions and devices on the substrate, as shown in Fig. 1 (b). To create the rectangular prism shaped ramp-down focusing electrode pairs, and the half 3D ellipsoid trapping electrode pairs, a micromold was patterned with a thickness of 15 μm.

The micromold was patterned using a thick layer of photoresist (AZ4620). The photoresist was spin coated, soft baked at 95 °C for 4 min, developed using AZ400k, and washed with DI water. We have then electroplated gold until the micromold was filled, using gold electroplating solution (Technic gold 25 ES solution). The solution was heated at 54 °C and stirred at 75 RPM. To achieve a thickness of 15 μm, a current of 50 nA was applied for 6 h. The micromold was then removed using acetone and isopropanol (IPA), the Cr thin film was etched using Chromium etchant (sigma aldrich) and washed with DI water Fig. 1(b).

The fluidic microchannel was patterned with a thickness of 50 μm using a negative photoresist (SU8-2050), which was spin coated at 3000 RPM for 30 s, prebaked at 65 °C for 2 min and then at 95 °C for 6.5 min, exposed with UV light for 8 s, post baked at 65 °C for 1.5 min and at 95 °C for another 5.5 min, developed for 1 min, and hard baked at 150 °C for 30 min. Next, the microfluidic channel was sealed using a PDMS slab. The PDMS was mixed with a curing agent thoroughly inside a plastic bag and poured into a petri dish with pre-fixed fluidic connectors, with glue, at locations corresponding to the inlets and outlets. The PDMS was left to cure overnight (>24 h). The PDMS was then cut into two rectangular slabs. The fluidic connectors were removed from one of the two PDMS slabs, exposed to oxygen plasma, and spin coated with a SU-8 2005 layer with a thickness of 3 μm. It was then baked at 95 °C for 10 min, aligned manually, and bonded to the glass.

substrate, and baked at 50 °C for 10 min on a hotplate while a weight of 4 kg was placed on top of the PDMS slab to improve the bonding strength. The second PDMS slab was exposed to oxygen plasma and bonded to the first PDMS layer manually. The PCB board was then patterned and etched with large copper (Cu) bonding pads, and the fabricated biosensors were fixed on the PCB board and wire bonded using silver epoxy. Scanning electron micrographs (SEMs) are shown in Fig. 1 (c).

2.4. Antibody preparation

Anti-SARS-CoV-2 ferret polyclonal antibody was used as the capture antibody. IgG was purified from the polyclonal ferret anti-SARS-COV-2 serum using a Pierce Protein A/G Chromatography Cartridge (Thermo Scientific, Cat#89930), and concentrated by using a 10 k Ultra-0.5 Centrifugal Filter Unit (MilliporeSigma, Cat#UFC510096). The purified polyclonal antibody original concentration was determined using the Quant-iT Protein Assay Kit with the working stock concentration of 1.8 mg/mL. As a negative control, IgG from the anti A/Switzerland/9715293/2013 (H3N2) specific ferret polyclonal antiserum (Ab SWZ/13) was purified in the same way with a working stock concentration of 3.72 mg/ml.

To improve the adhesion of the antibody to the gold electrode which is the detection area located on the surface of the IDE array, our previous study used cross-linker, sulfosuccinimidyl 6-[3-(2-pyridyldithio) propionamido] hexanoate (Sulfo-LC-SPDP) to immobilize the antibody to our device [16] and obtained effective signal response. In this study, we first combined the purified antibody with Sulfo-LC-SPDP (25 μL of 20 mM SPDP solution every 2 mg antibody), then removed extra cross-linker by dialysis (Slide-A-Lyzer Dialysis Cassette, Cat# 66383) to exclude potential false signal responses from non-specific binding. The final concentration of antibody was then determined by Quant-iT Protein Assay Kit (1.66 mg/ml). The antibody was then diluted and tested at various concentrations between 0.0166 and 1.66 mg/ml.

Before being immobilized on gold electrode, 5 μl thiolated antibody was incubated with 1.67 μl DTT (150 mM, pH7.0) for 30 min at room temperature to remove extra disulfide bonds from antibody. Subsequently, the thiolated antibody and DTT mixture experienced 10-fold dilution before immobilized on the gold surface of the IDE array. We also used second IDE array without antibody immobilization as a

Table 1
Clinical samples used in this study. The concentrations listed are the original concentration of the samples. Human nasopharyngeal or nasal swab samples were inactivated before being loaded on antibody coated biosensor. 100 mL of each wastewater sample was concentrated to a volume of 700 μl to 1 ml 500 μl viral eluent, which was then used for biosensor detection.

Sample	Sample ID	Collection date	RNA concentration (copies/ml)
Human clinical swab	Sample 1	Aug. 2020	5.88×10^{12}
	Sample 2	Aug. 2020	3.63×10^{6}
	Sample 3	Aug. 2020	7.67×10^{8}
	Sample 4	Aug. 2020	5.43×10^{6}
	Sample 5	Aug. 2020	7.08×10^{9}
	Sample 6	Aug. 2020	2.37×10^{8}
Wastewater	Sample 7	July 6th, 2020	4.32×10^{3}
	Sample 8	July 27th, 2020	1.31×10^{3}
	Sample 9	Aug. 10th, 2020	2.71×10^{3}
	Sample 10	Aug. 17th, 2020	1.61×10^{3}
	Sample 11	Aug. 17th, 2020	1.17×10^{3}
	Sample 12	June 23rd, 2020	1.15×10^{3}
	Sample 13	July 8th, 2020	1.17×10^{3}
	Sample 14	July 16th, 2020	1.62×10^{3}
	Sample 15	July 17th, 2020	1.00×10^{3}

control.

2.5. Sample preparation

Viruses: SARS-CoV-2 viruses were propagated in Vero E6 cells (CRL-1586, ATCC) at 37 °C with 5% CO_2 for 72 h. For viral titration, the 50% tissue culture infection dose (TCID50/ml) was determined on Vero E6 cells. Briefly, viruses were serially diluted on a 96-well plate and cultured with Vero E6 cells with a final concentration of 2×10^4/well at 37 °C in 5% CO_2. Cytopathic effects (CPE) were observed and recorded at 72 h post-infection (hpi).

To inactivate the viruses, formalin was added to viruses and made the final formalin concentration to 0.1%, which then incubated at 37 °C for 24 h. During method establishment, Figs. 1 and 2, we 10-fold serially diluted inactivated viruses into various concentrations with phosphate buffer saline (PBS). 500 μL of viruses were used for each test and three repeats were performed for each experimental condition.

Clinical samples: The human nasopharyngeal or nasal swab samples were collected from COVID-19 patients in the summer of 2020. These deidentified samples were inactivated with formalin as described above and diluted 1:10 in PBS before testing. A 10-fold dilution of inactive samples was executed before been loaded on the device. A total amount of 500 μL of each sample was then loaded into biosensors via suction at a flow rate of 3 μl/min, from the waste outlet, with the IDE array electrodes coated with the appropriate antibody.

Wastewater samples: Considering the technical application on SARS-CoV-2 surveillance in communities, we collected wastewater samples from Columbia, Missouri in April 2020 when COVID-19 cases were very

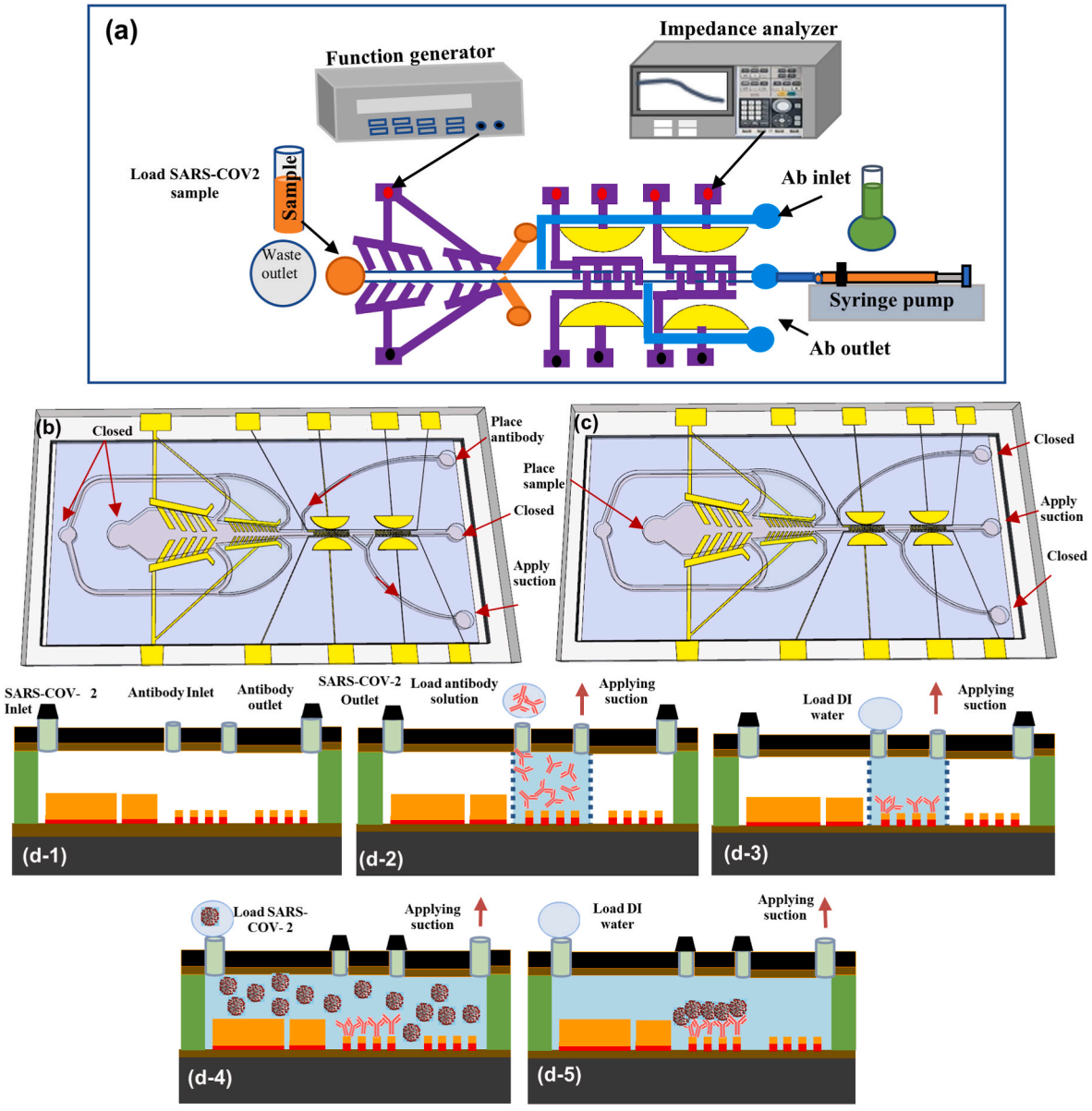

Fig. 3. (a) A schematic of the device testing setup showing. Top view schematics of the biosensor showing the solution flow direction during (b) antibody coating where the antibody-cross linker mixture was first placed at the antibody inlet and suction was applied to the antibody outlet while all other inlets were closed, (c) SARS-CoV-2 virus antigen sample was placed at the sample inlet while suction was applied to the sample outlet directing the flow toward the focusing region. The flow subsequently continued toward the detection region. (d) Process flow for antibody immobilization, and the antibody/antigen binding on the IDE array, (d-1) sideview of the device, (d-2) the antibody was loaded from the antibody inlet while suction was applied from the antibody outlet. All other inlets and outlets are closed, (d-3) the microchannel was washed after adhesion of antibody to the IDE array, (d-4) the virus sample was loaded into the sample inlet while suction was applied to the sample outlet, (d-5) the microchannel was washed again after antibody antigen binding was completed.

low, and in the summer of 2020 when the COVID-19 cases peaked (Table 1). 100 ml of wastewater samples were concentrated to 1 mL volume by a microbial collection and concentration system (SP select system, Innova Prep). The running condition of concentration was: "Ultra Protocol", 25% of pump speed, Ultrafilter (Cat. #: SKU CC08003-10), Tris elution fluid (Cat. #: SKU HC08001). 500 μl of these concentrated wastewater samples were used for tests.

2.6. Virus mRNA transcription level determination

The correlation between TCID50/ml titration and the RNA copies of SARS-CoV-2 virus was determined by quantitative reverse transcription PCR (qRT-PCR). Briefly, virus was subjected to was 10-fold serial dilution. The RNA of viruses with different concentration were extracted and purified from 200 μl dilutions and finally finished in 50 μl eluant. 2 μl of RNA eluant was used to qRT-PCR running. Primer and probe used in this experiment were from SARS-CoV-2 RUO qPCR Primer & Probe Kit (IDT, Cat#10006713). In this experiment, we detected N1 and N2 RNA levels. For the final calculation, we used the mean of N1 and N2 as the total RNA level of viruses.

2.7. Data analysis

The TCID50/ml was calculated by Reed-Muench Method [15] based on observed CPE. In order to unify the detection wastewater, we converted the RNA quantities to copies per milliliter.

2.8. Experimental setup

To test the biosensor, we first coated one set of IDE array with SARS-CoV-2 specific polyclonal antibody cross linker mixture against SARS-CoV-2 antigen. The antibody-cross linker mixture was first placed at the antibody inlet while suction was applied to the antibody outlet while all other inlets were closed, as shown in Fig. 3(b). The antibody suction was performed using a syringe pump (Harvard Apparatus PHD 2000) for 2 min until the flow showed up at the waste outlet to ensure that the sensing microchannel is filled with solution. The flow was then stopped for 60 min to allow the antibody to non-specifically adsorbed to the gold surface of the IDE array. The microchannel was then washed using distilled water to remove any unbounded antibodies and contaminants, as shown in Fig. 3(b). The antibody impedance was measured using an Impedance Analyzer (Keysight E4990A) from 100 Hz to 10 MΩ. The impedance testing set up is shown in Fig. 3(a). To confirm the accuracy of measurements, the same experiment, for each tested sample and concentration, was repeated 3 times. Each biosensor was used one sample and only once and was treated as disposable device.

The results from qRT-PCR revealed the correlation between propagated SARS-CoV-2 virus TCID50/mL titer and RNA was at a ratio $1{:}9.05 \times 10^5$, which means 1 TCID 50/ml correlated to 9.05×10^5 RNA copies of SARS-CoV-2 viruses.

We have tested PBS samples as well as wastewater samples spiked with various concentrations of SARS-CoV-2. We have also tested clinical human samples with various concentrations from 3.63×10^5 RNA copies/ml to 5.88×10^{11} RNA copies/ml. The impedance testing set up is shown in Fig. 3(a). The exact virus concentration in each human clinical samples were measured and validated using qRT-PCR. The

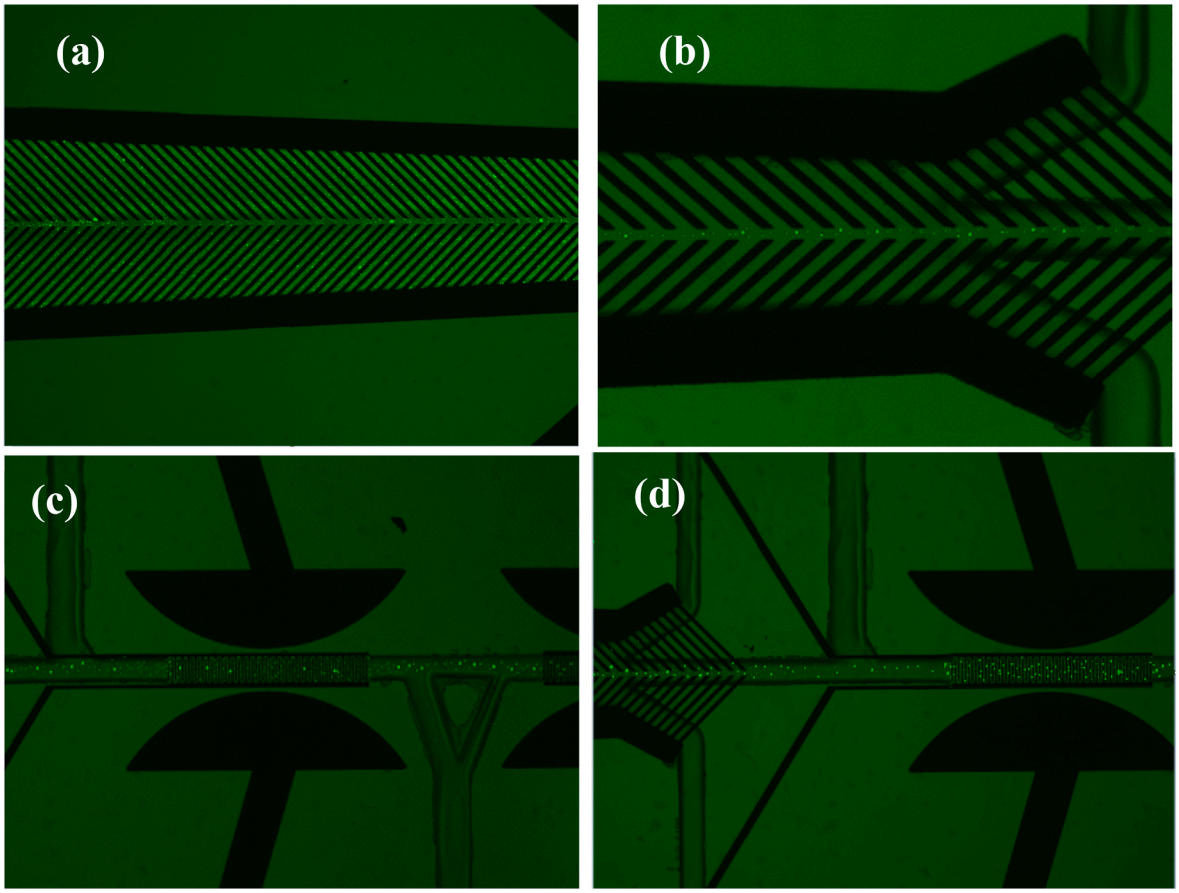

Fig. 4. (a) fluorescent images before focusing the nanobeads into the centerline of the focusing region, (b) fluorescent images after focusing the nanobeads into the centerline of the focusing region. (c) fluorescent images before trapping the nanobeads onto the surface of the detection electrode array. (d) fluorescent images after trapping the nanobeads onto the surface of the detection electrode array.

SARS-CoV-2 sample was placed at the sample inlet while suction was applied to the sample outlet directing the flow toward the focusing region (See Fig. 3 c). A function generator (Tektronix 3390) was connected to the electrode pairs and turned on with an optimized AC voltage and frequency to generate a positive p-DEP forces pushing the virus antigen toward the centerline of the microchannel. The fluid that is free of virus continued to flow toward the outer microchannels into the waste outlets. The virus-enriched solution was then entered the trapping/sensing region, where the sensing electrode was coated with a specific antibody against SARS-CoV-2. The trapping electrode pairs were connected to a second function generator and were turned on with a specific AC voltage and specific frequency to generate DEP forces to maximize the number of trapped viruses on top of the sensing electrode array. When the channel was filled with the solution, the flow was stopped for 30 min, while the function generator was still turned on, so that virus antigen could bind to its specific antibody. After 30 min, any unbound particles or viruses were then washed away using sterile deionized water (short as DI water), as shown in Fig. 3(c). The impedance of antibody-antigen binding was measured again between 100 Hz and 10 MHz using the same Impedance Analyzer. The impedance of the virus alone was determined by subtracting the antibody impedance from the impedance after antibody-antigen binding. We have used an inverted microscope equipped with a CCD camera to observe and capture images of the fluid flow through the microchannel during each testing experiment.

2.9. Ethics statement

This study was performed under the Institutional Re- view Board (#2023844) and the Biosafety Level 3 (#20-14), in compliance with the Institutional Biosafety Committee of the University of Missouri-Columbia.

3.Results and discussions

3.1. Testing the concentration region

To demonstrate the biosensor's focusing and trapping capabilities, fluorescent dielectric latex nanobeads standard (Thermo Fisher Scientific) were used because they can be seen using optical or fluorescent microscopes, and their permittivity value is 2.49 [1], which is similar to that of the SARS-CoV-2. The nanobeads have diameters <0.5 μm suspended in water with a dilution of 5 μl: 1 ml. They were injected from the sample inlet toward the focusing region while an optimum AC signal of 4 Vp-p at 5 MHz was applied across the focusing electrode pairs to generate p-DEP forces pushing the nanobeads toward the centerline of the microchannel. Fluorescent images of the nanobeads were captured, by a fluorescent microscope (Zeiss Axiovert 200 M with Leica DFC290 color camera), before and after focusing and are shown in Fig. 4. The nanobead enriched solution was then entered the trapping/sensing

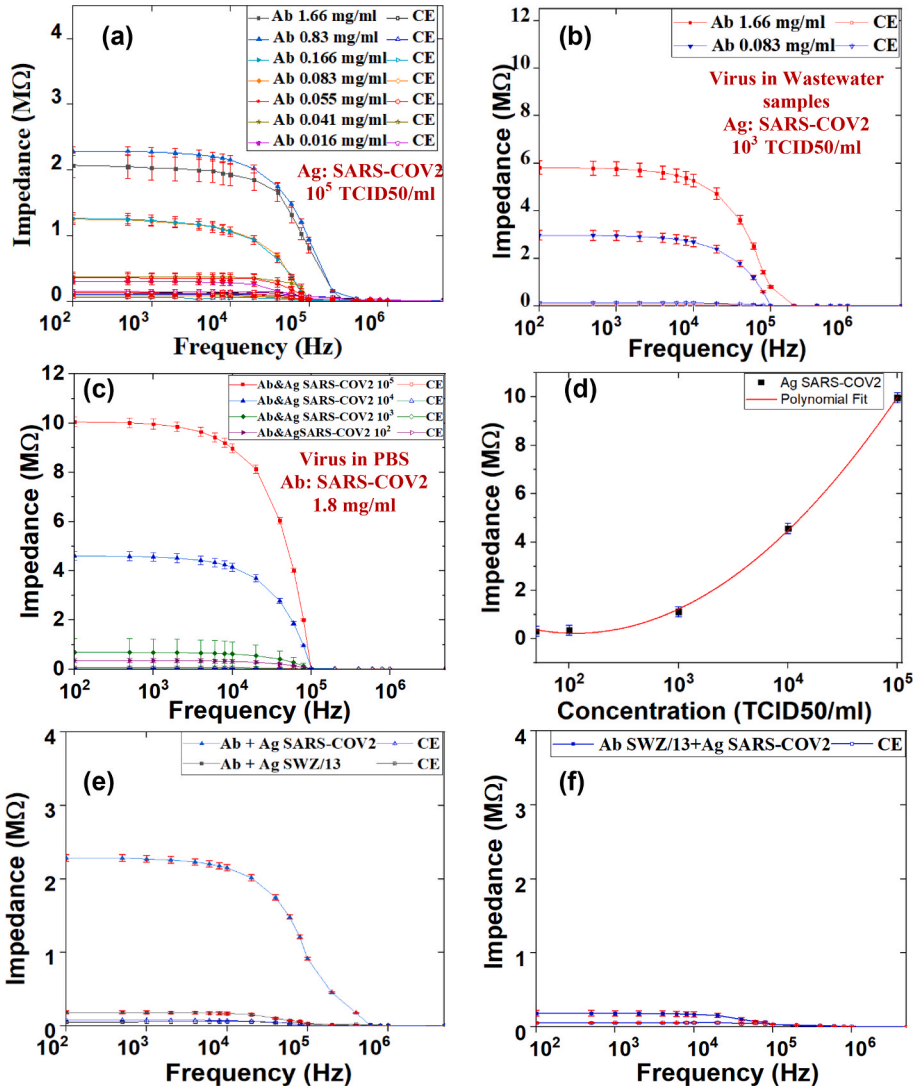

Fig. 5. (a) The optimal antibody concentration against SARS-CoV-2 virus was determined using multiple antibody dilutions from 0.0166 mg/ml to 1.66 mg/ml mixed with a cross linker (Sulfo-LC-SPDP). Each antibody dilution was tested using a fixed virus concentration at 105 TCID50/ml in PBS and a fixed antibody coating time, i.e., 60 min. (b) The optimal antibody concentration against SARS-CoV-2 virus was determined using wastewater samples spiked with fixed concentration of SARS-CoV-2, i.e., 10^3 TCID50/ml. (c) Testing of SARS-CoV-2 in PBS at various titers. (d) The impedance change was plotted versus antigen concentration at 1 kHz. (e) The specificity was tested by immobilizing antibody (Ab) SWZ/13 against influenza virus (1.3 μg/ml) on the sensing electrode while SARS-CoV-2 samples with a fixed concentration of 10^5 TCID50/ml in PBS were used. The result was compared with detection of the SARS-CoV-2 antigen using SARS-CoV-2 antibody for the same antigen concentration. (f) The selectivity was measured using influenza virus samples with a concentration of 10^6 TCID50/ml with the sensing electrode coated with SARS-CoV-2 antibody (0.083 mg/ml).

microchannel were another optimized AC voltage of 5 Vp-p at 6 MHz was applied to the trapping electrode pairs generating p-DEP forces which surface. Fluorescent images of the nanobeads before and after trapped the nanobeads on top of the sensing electrode trapping is shown in Fig. 4(a–d). These images demonstrated that the focusing and sensing regions were able to concentrate the nanobeads. Therefore, to concentrate the SARS-CoV-2, we have applied similar AC signals on the focusing and trapping electrodes. Although these alternating voltages may/may not provide an optimum value for concentrating the virus, they could be close enough due to the similarity of the permittivity values.

3.2. Testing antibody concentration

To determine the optimal polyclonal antibody concentration against SARS-CoV-2 virus, we have prepared multiple antibody dilutions from 0.0166 mg/ml to 1.66 mg/ml and mixed them with a cross linker (Sulfo-LC-SPDP). Each antibody dilution was tested using propagated inactivated SARS-CoV-2 virus at original concentration (9.05×10^{10} viral RNA/ml in PBS) and a fixed antibody coating time, i.e., 60 min. The sensing IDE array was coated with a specific antibody cross linker mixture, the microchannel was then washed using DI water for 15 min and the antibody impedance was measured as discussed in the experimental testing setup section Figs. 3 (d-2,3). Then, a SARS-CoV-2 sample (propagated virus spiked in PBS) at a concentration of 9.05×10^{10} RNA/ml was placed at the sample inlet and suction was applied, with a flow rate of 3 μl/min, from the sample outlet, making the sample flow toward the focusing electrode region Figs. 3(d-4). The virus antigens were concentrated at the centerline of the microchannel and continued to flow toward the sensing microchannel Figs. 3 (d-4). When the sensing microchannel was filled with the sample solution, the flow was stopped for 30 min, during which the antigen was allowed to bind with the antibody. The microchannel was then cleaned with DI water for 15 min and the impedance was measured again Figs. 3(d-5). The impedance of viruses alone was determined by subtracting the antibody impedance from the impedance after antibody-antigen binding. The impedance change was measured at 1 KHz plotted as a function of frequency for different antibody concentrations from 0.0166 mg/ml to 1.66 mg/ml, as shown in Fig. 5(a). The results demonstrated that the highest average impedance signal of ~2.2 MΩ was achieved with an optimal antibody concentration of 0.83 mg/ml. We also determined that the 0.166 mg/ml antibody provided a relatively statistic importance and acceptable average impedance value of 1.2 MΩ.

Wastewater-based epidemiology (WBE) has been successfully used in surveillant the spread of SARS-CoV-2 since the beginning of COVID-19 pandemic. It provides better understanding the virus prevalence in the communities [18]. Our goal to develop this device is to provide an alternative viral detection method thus further to contribute the SARS-CoV-2 virus surveillance. Towards the aim, we sought to mimic clinical application in the context of wastewater. We spiked inactivated SARS-CoV-2 at a concentration of 9.05×10^8 viral RNA/ml (equals to 1×10^3 TCID50/ml) into SARS-CoV-2 negative wastewater, which was collected in early April of 2020 when the cases were sparse in the communities, to define the optimized antibody concentration. We tested two antibody concentrations, 0.166 mg/ml and 0.083 mg/ml. Similar to the PBS viral background, in wastewater background, 0.166 mg/ml antibody provided a higher average impedance signal of ~5.8 MΩ, while 0.083 mg/ml antibody generated an acceptable average impedance value of 2.8 MΩ, as shown in Fig. 5(b).

Although a higher concentration of antibody displayed more statistic importance of impedance signal, in practice, detection cost is also an important consideration. Therefore, from experimental (in PBS) and clinical (in wastewater) background test results above, we utilized 0.083 mg/ml antibody as our optimized condition for the subsequent experiments.

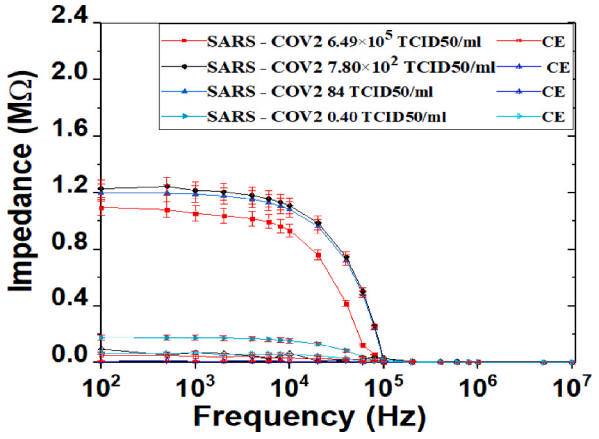

Fig. 6. Testing of Four inactivated clinical human samples with final various titrations between 0.40 and 6.49′10^5 TCID50/ml after 10-fold dilution.

3.3. Testing the sensitivity of the biosensor

To determine the biosensor sensitivity i.e., the lowest measurable concentration (LOD), original concentration of SARS-CoV-2 virus was diluted with PBS to achieve various viral RNA concentrations from 9.05×10^{11}/ml to 9.05×10^7/ml. The samples were then placed at the sample inlet and sucked into biosensors from the sample outlet with first IDE array coated with the appropriate antibody at a 9.05×10^{11}/ml to 9.05×10^7. The second electrode was used as a control electrode and was not coated or contaminated with the antibody. The impedance changes across the sensing electrode array and the control electrode array resulting from the binding of the virus antigen were measured from 10 Hz to 10 MHz using an impedance analyzer. The antibody coating and virus sample introduction were discussed in the experimental testing setup section. It is noted that the antibody coating time and antigen binding time were 60 min and 30 min, respectively. Each washing step lasted for 15 min. The results were plotted in Fig. 5(c) and demonstrated that the detection electrode that has matching antibody to the antigen showed strong impedance change while the control electrode showed weak signals concentration of 0.083 μg/ml. The impedance changes as a function of antigen concentration measured at 1 kHz and plotted in Fig. 5(d). Viral RNA concentrations from confirming the signal was correct. The biosensor sensitivity, i.e., the lowest measured concentration (LoD) of the SARS-CoV-2 antigen was 4.52×10^7 copies/ml. The changes of the impedance of the. control electrode array for PBS samples were very small confirming the accuracy of the measurements.

3.4. Testing the specificity and selectivity of the biosensor

To confirm the specificity of the biosensor, the antibody (Ab) anti-SWZ/13 was diluted to 0.083 mg/ml and then immobilized on the sensing electrode while SARS-CoV-2 samples with a fixed concentration of 105 TCID50/ml (correlated to 9.05×10^{10} RNA copies/ml) in PBS were tested as an antigen. The measured response of the influenza antibody showed no difference in the impedance measurement values with respect to the baseline impedance (antibody value) response of the IDE array while the measured response using SARS-CoV-2 antibody shows a strong signal confirming the specificity of the biosensor. In addition, the control electrode impedance change was almost zero. Fig. 5(e) showed the specificity results along with the results for sensing the SARS-CoV-2 antigen using SARS-CoV-2 antibody for similar antigen concentration.

To measure the specificity of the biosensor, influenza virus samples with a concentration of 10^6 TCID50/ml (correlated to 10^9 RNA copies/

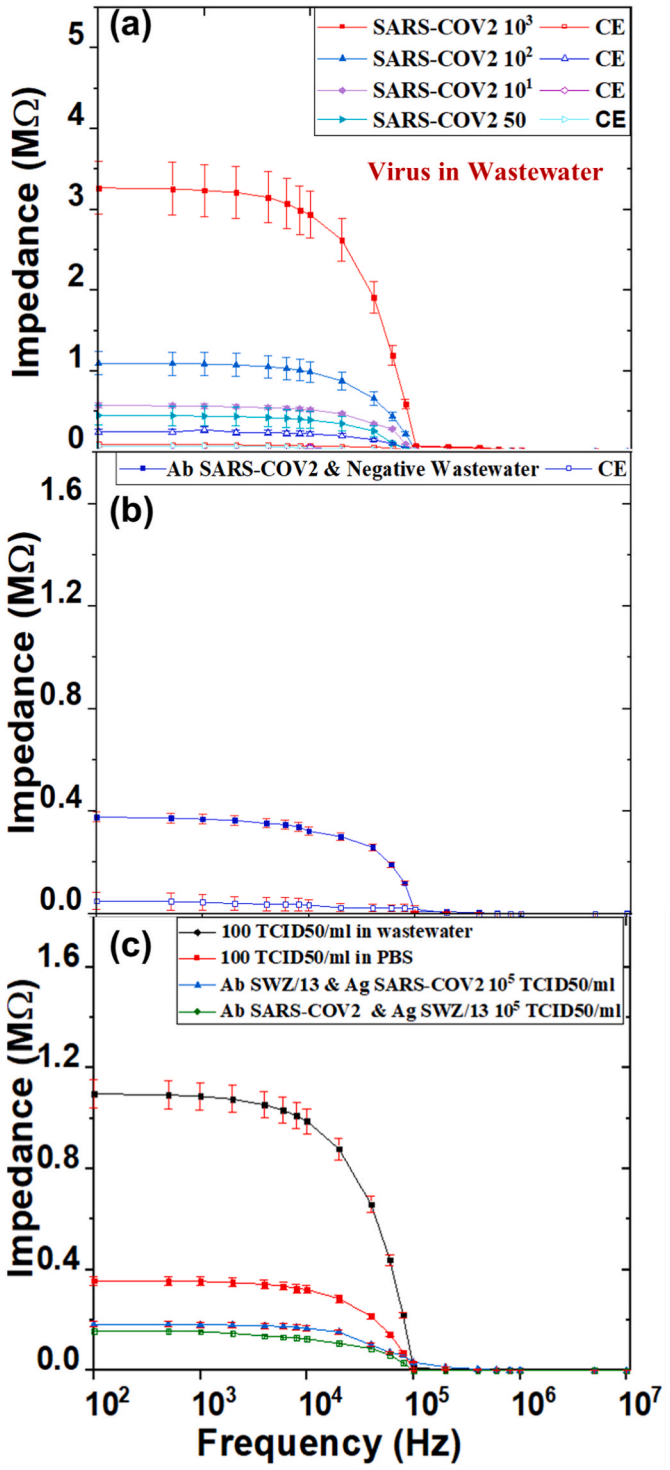

Fig. 7. (a) wastewater samples were spiked with various concentration (50-10^3 TCID50/ml) of SARS-CoV-2, (b) wastewater samples that were collected in April 2020. They were tested negative for SARS-CoV-2. (c) comparison between the results of testing a low concentration of SARS-CoV-2 in PBS (100TCID50/ml), and in wastewater (100 TCID50/ml), and non-specific binding of SARS-CoV-2 with high concentrations (10^5 TCID50/ml) to influenza antibody, and non-specific binding of Influenza with high concentrations (10^5 TCID50/ml) to SARS-CoV-2 antibody.

ml) were tested with the sensing electrode coated with SARS-CoV-2 antibody (0.083 mg/ml). The measured response of influenza showed a weak impedance signal, i.e., comparable to the baseline impedance (antibody value) response of the IDE array, confirming the selectivity of the biosensor. In addition, the control electrode impedance change was almost zero. Confirming the accuracy of the measurements. Fig. 5(f) shows the impedance measurement of the influenza antigen.

3.5. Testing clinical samples

Four inactivated clinical human swab samples with various viral RNA levels between 3.63×10^6–5.88×10^{12} copies/ml were tested using the same procedures discussed to determine the biosensor sensitivity. Prior to testing, the samples were subjected to 10-fold dilution. The testing results showed that the 4 diluted samples with final concentrations between 2.37×10^7 and 5.88×10^{11} RNA copies/ml were tested positive while 2 diluted samples with final concentrations of 3.63×10^5 and 5.43×10^5 RNA copies/ml were tested negative. This is due to their low virus concentrations. Therefore, the results indicate as low as 2.37×10^7 RNA copies/ml could be detected by our biosensor device. The clinical swabs to be used in the assays are processed as the same way as those used in rapid diagnosis, and no specific procedures are needed. In fact, all the clinical swabs are from those samples collected for diagnosis, and we simply used an aliquot for this study.

The non-autoclaved SARS-CoV-2 mock control wastewater was collected in April 2020 and had a pH 7. Multiple samples were tested without being autoclaved and confirmed negative status for SARS-CoV-2 antigen via qPCR testing (See Fig. 6). The SARS-CoV-2 antigen was spiked into the wastewater samples without autoclaving or any other treatment to obtain multiple concentrations of samples, from 50 to 10^3 TCID50/ml (correlated to 4.52×10^7 copies/ml to 9.05×10^8) copies/ml. Both the positive and negative controls were tested using the same antibody and same procedure that was used for testing the virus in PBS samples, discussed in the sensitivity testing section. Fig. 7(a) shows the impedance change of the wastewater samples with various virus antigen concentrations. The results demonstrated the biosensor was able to detect SARS-CoV-2 antigen in complex samples at low concentration (50 TCID50/ml or 4.52×10^7 RNA copies/mL) the impedance was 0.451 MΩ while the impedance of the negative control electrode was 0.072 MΩ. The changes of the impedance of the negative control electrode array were very small. confirming the accuracy of the measurements. We sought to apply our device on community virus surveillance, toward this end, we received wastewater samples from different sites of Missouri during pandemic and tested in the biosensor. However, we couldn't get obvious impedance signal from them (date not shown).

Technicians becomes the bottleneck of the widespread of this technology. Conventional antigen test is inexpensive, which do not need clinical sample s to be processed prior to testing. More importantly, antibodies used in antigen test are manufactured in advance at the manufacturer and pre-loaded into the test kit, thus greatly reduce the testing time. Although there are several antigen test kits available in the market, our device (biosensor) is a different antigen based viral sensor with unique mechanism compared to other products in the market. Instead of visible antibody result (strip) in the detection area of positive samples, the viral detection signal reflects in impedance changes, which provides a perspective to the alternative antigen detection method. The detection process needs approximately 30 min, and acceptable sensitivity is available. Based on the principle of our device, the biosensor could be further used in other pathogen detections with minor changeable settings.

It has been known that COVID patients typically developed diseases after 2–14 incubation period, and the patients usually shed viruses from 5 to 21 days after disease onset. The patients can shed at least 100 TCID50/ml from Day 1 (disease onset), and more than 10^6 TCID50/ml during the peaking time. Our device achieved a sensitivity in detecting viruses at 50 TCID50/ml (4.52×10^7 RNA copies/ml), as allows us to

detect viruses at a very earlier date of disease onset. Thus, this device provides an alternative approach for rapid diagnosis for COVID patients. Different from RAT which requires monoclonal antibody (mAb), we used polyclonal antibody as the antibody resource in our device. Compared with mAb, a polyclonal antibody is much easier to be prepared. More important, polyclonal antibody has more tolerance for antigenic variations among the SARS-CoV-2, and thus can catch the emerging variants during the diagnosis. As a future study, we will aim to develop our device to detect antigenic variants by using a panel of polyclonal antibodies against different variants.

Due to the low viral loads in the wastewater, which is typically approximately 10^3 RNA copies/mL, our device is not yet sensitive enough to detect viruses in wastewater samples. We plan to optimize the antigen catching in our device to improve the antigen catch so that we can increase the antigen concentration. In addition, we can improve our methods to concentrate the viral agents directly from the water before loading to our device.

Another limitation in this study is that we only included the limited number of clinical samples ($n = 6$). We noticed that the viral titer (TCID50) of the detectable sample corresponding to the lowest RNA level is lower than our TCID50 detection line in PBS. Other investigators suggest that the viral titer to RNA ratio varies among variants [20]. Thus, it is possible that the individual human samples bring variation of viral titer to RNA ratio versus cell cultured virus. We plan to apply more clinical samples to optimize the detection line in application. Nevertheless, since it is the first generation of biosensor to detect SARS-CoV-2 virus, we will continue improve the sensitivity and develop high throughput devices in the future study.

4. Conclusion

An impedance-based microfluidic MEMS biosensor was investigated for rapid detection of SARS-CoV-2 antigen in

clinical human samples. The biosensor was designed for one-time use, as a disposable device for use in-field for clinical settings or in laboratories. The biosensor can be used for the detection of a wide range of viruses such as influenza, dengue, and Zika in humans and animals.

The device sensitivity was demonstrated by testing PBS as well as wastewater samples spiked with a known concentration of SARS-CoV-2 antigen. A combination of focusing electrode pairs and trapping electrode pairs were used to increase the virus concentration available for binding with the antibody in order to increase the sensitivity. One set of IDE arrays was used for SARS-CoV-2 antigen detection and another set was used for control to confirm the accuracy of the testing results. The biosensor was tested successfully in the presence of various dilutions of positive antigen samples, and positive clinical human samples from 100 Hz to 10 MHz. The biosensor was able to detect SARS-CoV-2 antigen in clinical human samples with a dilution as low as 26 TCID50/ml in 40 min.

Author contributions

S.A. Modeling and simulation, mask design, fabrication, investigation, validation, data curation and analysis, Writing – original draft, Writing – review & editing; Y.H. Sample preparation, data curation and analysis, Writing – review & editing; M.A. contributed to fabrication, contributed to modeling and simulation; K.S. Sample preparation, Writing – review & editing; A.A. contributed to fabrication; Y.W. Sample preparation, Writing – review & editing; O.A. contributed to fabrication; R.H. Methodology, Data analysis and interpretation Project administration; G.H. Methodology, Data analysis and interpretation Project administration; Z.E. Methodology, Data analysis and interpretation, Project administration; R.P. Methodology, Data analysis and interpretation Project administration; G. H. Methodology, Data analysis and interpretation Project administration; X.W. Conceptualization, Funding acquisition, Methodology, Project administration, Resources, Supervision, Writing – original draft, Writing – review & editing; M.A. Conceptualization, Funding acquisition, Methodology, Project administration, Resources, Supervision, Writing – original draft, Writing – review & editing.

Declaration of competing interest

The authors declare that they have no known competing financial interests or personal relationships that could have appeared to influence the work reported in this paper.

Data availability

Data will be made available on request.

Acknowledgments

This project was funded by Black and Veatch. We acknowledge Drs Xiaojiang Zhang and Minhui Guan for their technical assistance in this project, and Dr. Jane McElroy, Naser Ashiekh, and Cynthia Tang for their assistance in acquiring and de-identifying human clinical samples. We are grateful for Erin Keys, George Gering, Hannah Langbart, and Tami Hansen from Columbia City Sanitary Sewer and Storm Water Utilities of City for their assistance in collecting water samples used in this study. The first two authors have equal contributions in the experiment. The last two authors (corresponding authors) have equally contributed.

References

[1] P. Zhou, X.-L. Yang, X.-G. Wang, B. Hu, L. Zhang, W. Zhang, H.-R. Si, Y. Zhu, B. Li, C.-L. Huang, H.-D. Chen, J. Chen, Y. Luo, H. Guo, R.-D. Jiang, M.-Q. Liu, Y. Chen, X.-R. Shen, X. Wang, X.-S. Zheng, K. Zhao, Q.-J. Chen, F. Deng, L.-L. Liu, B. Yan, F.-X. Zhan, Y.-Y. Wang, G.-F. Xiao, Z.-L. Shi, A pneumonia outbreak associated with a new coronavirus of probable bat origin, Nature 579 (2020) 270–273, https://doi.org/10.1038/s41586-020-2012-7.

[2] E.M. Leroy, M. Ar Gouilh, J. Brugère-Picoux, The.

[3] Y. Zhang, X. Geng, Y. Tan, Q. Li, C. Xu, J. Xu, L. Hao, Z. Zeng, X. Luo, F. Liu, H. Wang, New understanding of the damage of SARS-CoV-2 infection outside the respiratory system, Biomed. Pharmacother. 127 (2020), 110195, https://doi.org/10.1016/J.BIOPHA.2020.110195.

[4] H. Wang, K.R. Paulson, S.A. Pease, S. Watson, H. Comfort, P. Zheng, A.Y. Aravkin, C. Bisignano, R.M. Barber, T. Alam, J.E. Fuller, et al., Estimating excess mortality due to the COVID-19 pandemic: a systematic analysis of COVID-19-related mortality, 2020–21, Lancet 399 (10334) (2022) 1513–1536, https://doi.org/10.1016/S0140-6736(21)02796-3.

[5] World Health Organization, WHO coronavirus (COVID19) dashboard coronavirus (COVID-19) dashboard [Internet].[consultado 25 Sep 2021]. https://covid19.who.int/. (Accessed 7 April 2022).

[6] Sandip Mandal, Nimalan Arinaminpathy, Balram Bhargava, Samiran Panda, Plausibility of a third wave of COVID-19 in India: a mathematical modelling based analysis, Indian J. Med. Res. 153 (5–6) (2021) 522–532, https://doi.org/10.4103/ijmr.ijmr_1627_21.

[7] O. Filchakova, D. Dossym, A. Ilyas, T. Kuanysheva, A. Abdizhamil, R. Bukasov, Review of COVID-19 testing and diagnostic methods, Talanta 244 (2022), 123409, https://doi.org/10.1016/J.TALANTA.2022.123409.

[8] COVID-19 Test Basics | FDA, (n.d.). https://www.fda.gov/consumers/consumer-updates/covid-19-test-basics (accessed April 7, 2022).

[9] L.M. Kucirka, S.A. Lauer, O. Laeyendecker, D. Boon, J. Lessler, Variation in false-negative rate of reverse transcriptase polymerase chain reaction–based SARS-CoV-2 tests by time since exposure, Ann. Intern. Med. 173 (2020) 262–268, https://doi.org/10.7326/M20-1495/SUPPL_FILE/M20-1495_SUPPLEMENT.PDF.

[10] S.A. El-Kafrawy, M.M. El-Daly, A.M. Hassan, S.M. Harakeh, T.A. Alandijany, E. I. Azhar, Rapid and reliable detection of SARS-CoV-2 using direct RT-LAMP, Diagnostics 12 (2022) 828, https://doi.org/10.3390/DIAGNOSTICS12040828.

[11] T. Shaffaf, E. Ghafar-Zadeh, COVID-19 diagnostic strategies. Part I: nucleic acid-based technologies, Bioengineering 8 (49) (2021), https://doi.org/10.3390/BIOENGINEERING8040049.

[12] S.D. Bukkitgar, N.P. Shetti, T.M. Aminabhavi, Electrochemical investigations for COVID-19 detection-A comparison with other viral detection methods, Chem. Eng. J. 420 (2) (2021), 127575, https://doi.org/10.1016/J.CEJ.2020.127575.

[13] S. Stanley, D.J. Hamel, I.D. Wolf, S. Riedel, S. Dutta, E. Contreras, C.J. Callahan, A. Cheng, R. Arnaout, J.E. Kirby, P.J. Kanki, Limit of detection for rapid antigen testing of the SARS-CoV-2 omicron and delta variants of concern using live-virus culture, Clin. Microbiol. 60 (5) (2022), https://doi.org/10.1128/JCM.00140-22, 001400-e222.

[14] J.N. Kanji, N. Zelyas, C. MacDonald, K. Pabbaraju, M.N. Khan, A. Prasad, J. Hu, M. Diggle, B.M. Berenger, G. Tipples, False negative rate of COVID-19 PCR testing: a discordant testing analysis, Virology 18 (2021) 1–6, https://doi.org/10.1186/S12985-021-01489-0/TABLES/3.

[15] S. Fafi-Kremer, T. Bruel, Y. Madec, R. Grant, L. Tondeur, L. Grzelak, I. Staropoli, F. Anna, P. Souque, S. Fernandes-Pellerin, N. Jolly, C. Renaudat, M.N. Ungeheuer, C. Schmidt-Mutter, N. Collongues, A. Bolle, A. Velay, N. Lefebvre, M. Mielcarek, N. Meyer, D. Rey, P. Charneau, B. Hoen, J. De Seze, O. Schwartz, A. Fontanet, Serologic responses to SARS-CoV-2 infection among hospital staff with mild disease in eastern France, EBioMedicine 59 (2020), 102915, https://doi.org/10.1016/J.EBIOM.2020.102915.

[16] M. Yüce, E. Filiztekin, K.G. Özkaya, COVID-19 diagnosis —a review of current methods, Biosens. Bioelectron. 172 (2021), 112752, https://doi.org/10.1016/J.BIOS.2020.112752.

[17] J. Liu, I. Jasim, A. Abdullah, Z. Shen, L. Zhao, M. El-Dweik, S. Zhang, M. Almasri, An integrated impedance biosensor platform for detection of pathogens in poultry products, Sci. Rep. 8 (1) (2018), 16109, https://doi.org/10.1038/s41598-018-33972-0.

[18] S. Eissa, M. Zourob, Development of a low-cost cotton-tipped electrochemical immunosensor for the detection of SARS-CoV-2, Cite This: Anal. Chem. 93 (2021) 1826–1833, https://doi.org/10.1021/acs.analchem.0c04719.

[19] L.T. Allan-Blitz, J.D. Klausner, A real-world comparison of SARS-CoV-2 rapid antigen testing versus PCR testing in Florida, Clin. Microbiol. 59 (10) (2021), e01107-e01121, https://doi.org/10.1128/JCM.01107-21.

[20] M. Alafeef, K. Dighe, P. Moitra, D. Pan, Rapid, ultrasensitive, and quantitative detection of SARS-CoV-2 using antisense oligonucleotides directed electrochemical biosensor chip, ACS Nano 14 (12) (2020) 17028–17045, https://doi.org/10.1021/acsnano.0c06392.

[21] Y. Yuan, T. Guo, X. Qiu, J. Tang, Y. Huang, L. Zhuang, S. Zhou, Z. Li, B.-O. Guan, X. Zhang, J. Albert, Electrochemical surface plasmon resonance fiber-optic sensor: in situ detection of electroactive biofilms, Anal. Chem. 88 (15) (2016) 7609–7616, https://doi.org/10.1021/acs.analchem.6b01314.

[22] M.U. Hadi, M. Khurshid, SARS-CoV-2 detection using optical fiber based sensor method, Sensors 22 (3) (2022) 751, https://doi.org/10.3390/s22030751.

[23] S. Tripathy, · Shiv, G. Singh, Label-free electrochemical detection of DNA hybridization: a method for COVID-19 diagnosis, Trans. Indian Nat. Acad. Eng. 5 (2) (2020) 205–209, https://doi.org/10.1007/s41403-020-00103-z.